JOURNAL OF GEOPHYSICAL RESEARCH, VOL. 112, C06023, doi:10.1029/2006JC003946, 2007

Modeling of upwelling/relaxation events with the Navy Coastal Ocean Model

Igor Shulman,[1] John Kindle,[1] Paul Martin,[1] Sergio deRada,[2] Jim Doyle,[3] Brad Penta,[1] Stephanie Anderson,[1] Francisco Chavez,[4] Jeff Paduan,[5] and Steve Ramp[5]

Received 27 September 2006; revised 6 February 2007; accepted 28 March 2007; published 26 June 2007.

[1] The Navy Coastal Ocean Model (NCOM) is a free-surface, primitive-equation model that is under development at the Naval Research Laboratory (NRL). The NCOM-based model of the Monterey Bay area is evaluated during a series of upwelling and relaxation wind events in August–September of 2000. The model receives open boundary conditions from a regional NCOM implementation of the California Current System and surface fluxes from the Navy Coupled Ocean/Atmosphere Mesoscale Prediction System (COAMPS^{TM})(COAMPS is a registered trademark of the Naval Research Laboratory). Issues investigated in this study are: NCOM-based model simulations of upwelling and relaxation events, coupling to COAMPS, use of sigma versus hybrid (sigma-*z*) vertical grids, and coupling with a larger-scale model on the open boundaries. The NCOM simulations were able to reproduce the observed sequence of the upwelling and relaxation events, which can be attributed, in part, to the good agreement between the observed and COAMPS winds. Comparisons with the mooring observations show that COAMPS overestimates shortwave radiation values, which makes the NCOM modeled SSTs too warm in comparison with observations. The NCOM runs forced with different resolution atmospheric forcing (3 versus 9 km) do not show significant differences in the predicted SSTs and mixed-layer depths at the mooring locations. At the same time, during the extended upwelling event, the model runs forced with 3 and 9 km resolution COAMPS fields show differences in the surface circulation patterns, which are the most distinct in the southern portion of the model domain. The model run with 9-km forcing develops a northward flow along the coast, which is not present in the run with 3-km forcing and in observations (for example, HF radar-derived radials). Comparison of the wind patterns of the 3- and 9-km products shows a weakening of the 9-km wind stress along the southern coast of the NCOM model domain, which is responsible for the development of the artificial northward flow in the NCOM run with 9-km forcing.

Citation: Shulman, I., J. Kindle, P. Martin, S. deRada, J. Doyle, B. Penta, S. Anderson, F. Chavez, J. Paduan, and S. Ramp (2007), Modeling of upwelling/relaxation events with the Navy Coastal Ocean Model, *J. Geophys. Res.*, *112*, C06023, doi:10.1029/2006JC003946.

1. Introduction

[2] A multi-institution, multidisciplinary field experiment was conducted in the Monterey Bay area during August–September of 2000 [*Ramp et al.*, 2005]. The experiment represented a joint effort of the Autonomous Ocean Sampling Network (AOSN I), the Monterey Bay Aquarium Research Institute (MBARI) Upper-Water column Science Experiment (MUSE), and the National Oceanic Partnership Program (NOPP) Innovative Coastal-Ocean Observing Network (ICON) projects. The experiment objectives ranged from a study and modeling of biophysical processes of the upwelling centers to the development of components of a real-time observational and modeling system for the Central California.

[3] The observational network consisted of a combination of airborne, in situ, AUVs, and shore-based HF radar observations, and the observational period (15 August–2 September) included an extended upwelling event during 15–21 August and an extended wind relaxation event from 28 August through 2 September. The numerical ocean model was based on the Princeton Ocean Model [POM, *Blumberg and Mellor*, 1987] of the Central California Coast

[1]Oceanography Division, Naval Research Laboratory, Stennis Space Center, Mississippi, USA.
[2]Jacobs Sverdrup, Stennis Space Center, Mississippi, USA.
[3]Marine Meteorology Division, Naval Research Laboratory, Monterey, California, USA.
[4]Monterey Bay Aquarium Research Institute, California, USA.
[5]Department of Oceanography, Naval Postgraduate School, Monterey, California, USA.

0148-0227/07/2006JC003946$09.00

developed under the ICON project [*Paduan and Shulman*, 2004; *Shulman et al.*, 2002].

[4] As noted in *Ramp et al.* [2005], the POM ICON model results were very consistent with observations during the upwelling event but differed significantly during the extended relaxation period. During the relaxation period, strong onshore translation of warmer California Current water combined with local surface heating inside the Bay resulted in extraordinary surface warming within the bay during 30–31 August. It was hypothesized by *Ramp et al.* [2005] that the model's difficulty in reproducing the extreme heating event was likely due to inaccuracies in both the wind stress and surface heat fluxes from the 9-km COAMPS and insufficient vertical resolution of the upper ocean in the model itself.

[5] The POM ICON model [used by *Ramp et al.*, 2005] is a three-dimensional, free-surface model with 1–4 km horizontal resolution and thirty-vertical sigma levels [*Shulman et al.*, 2002]. The model was forced with 9-km resolution wind stresses and heat fluxes from the Navy Coupled Ocean and Atmospheric Mesoscale Prediction System (COAMPS^{TM}) reanalysis for the US west coast [*Hodur et al.*, 2002; *Kindle et al.*, 2002] and by the regional Pacific West Coast (PWC) model [*Haidvogel et al.*, 2000; *Rochford and Shulman*, 2000] on the seaward boundaries. The model assimilated surface currents from HF radar (CODAR) sites around the Monterey Bay area [*Paduan and Shulman*, 2004].

[6] In the present paper, the Navy Coastal Ocean Model (NCOM) [*Rhodes et al.*, 2002; *Martin*, 2000] together with two new high-resolution COAMPS surface flux fields are utilized in order to evaluate the NCOM model's predictive capabilities and to examine the sensitivity of the simulated circulation patterns to the model formulation and surface forcing functions. The NCOM model is based on POM, but has options for using different turbulence closure, advection, and open boundary condition schemes, etc. The NCOM in Monterey Bay (noted below as NCOM ICON model) is set up on the same grid as the POM ICON. Since August of 2000, a number of modifications were made to the COAMPS, most important differences are the addition of a high-resolution 3-km nest and improvements to the surface flux scheme and microphysics parameterization.

[7] Models can provide us with additional information about circulation patterns and water mass properties and formations which can not be revealed by limited observations alone. The circulation patterns of the POM ICON model simulations [*Ramp et al.*, 2005] revealed distinct differences in the circulation and water mass properties of Monterey Bay during the upwelling and relaxation events. In the present paper, our objective is to continue the analysis of the circulation patterns and water mass properties predicted by the models of Monterey Bay.

[8] The paper has the following structure: In section 2, we describe the hierarchy of different resolution NCOM-based models in the Pacific Ocean used in this study. A description of the atmospheric forcing is presented in section 3. Section 4 provides a brief description of the physical conditions in the Bay during 2 weeks of August 2000 as well as an evaluation of COAMPS predicted surface fluxes. Section 5 presents an evaluation and analysis of the model results. This section is split into four subsections, which focus on the model sensitivity to the resolution of the atmospheric forcing and to the vertical coordinate system and simulations during the extended relaxation and upwelling events. Section 6 is devoted to discussion and conclusions.

2. Description of Hierarchy of NCOM-Based Different Resolution Models in the Pacific Ocean

[9] NCOM is a primitive-equation, three-dimensional, hydrostatic model [*Rhodes et al.*, 2002; *Martin*, 2000]. The model is based on POM, but has options for using different turbulence closure, advection, and open boundary condition schemes, etc. The model includes routines for direct reading and processing of atmospheric COAMPS fields. NCOM allows for the use of a sigma or hybrid sigma/z-level vertical coordinate systems. The code is parallelized and runs on many different computer platforms.

[10] To accommodate the wide range of horizontal scales of physical and biological oceanic processes, the Naval Research Laboratory (NRL) uses a hierarchy of different resolution, NCOM-based ocean models. The NCOM global model [*Rhodes et al.*, 2002] is run in real-time and uses a hybrid vertical coordinate system with 19 sigma layers from the surface down to 138-m depth and 21 z-levels between 138 m and the bottom. Global NCOM has 1/8° horizontal resolution, assimilates three-dimensional temperature and salinity observations derived from the Modular Ocean Data Assimilation System [MODAS; *Fox et. al.*, 2002], and uses atmospheric forcing from the Navy Global Atmospheric Prediction System [NOGAPS; *Rosmond et al.*, 2002].

[11] Global NCOM provides boundary conditions for an NCOM-based regional model of the California Current [NCOM CCS, *Shulman et al.*, 2004]. The NCOM CCS has a horizontal resolution of about 9 km and is used with two different vertical coordinate systems: (1) a purely sigma-coordinate grid with 30 layers, and (2) the same 40-layer, hybrid grid used in the global model. In the present study, the NCOM CCS with the hybrid (40-layer) vertical coordinate system is used. The NCOM CCS model is forced with atmospheric products derived from the COAMPS predictions [*Kindle et al.*, 2002]. As in the global model, the NCOM CCS assimilates three-dimensional temperature and salinity observations derived from the MODAS.

[12] NCOM CCS provides boundary values to the high-resolution NCOM ICON model of the Monterey Bay Area. The NCOM ICON runs on an orthogonal, curvilinear grid, which has a variable horizontal resolution ranging from 1 to 4 km, with finer resolution in and around Monterey Bay (Figure 1). The NCOM ICON is set up on the same horizontal grid as the POM ICON [*Shulman et al.*, 2002]. The model uses the Mellor-Yamada level 2.5 turbulence closure scheme [*Martin*, 2000]. In this study, the NCOM ICON is forced with atmospheric fluxes from COAMPS (no bulk formulations for heat fluxes or relaxation terms are used, see section 3). The MODAS derived temperature and salinity are not assimilated into the fine-resolution NCOM ICON model.

3. Atmospheric Forcing

[13] The atmospheric fields from two COAMPS versions (COAMPSv2 and COAMPSv3) are used in this study. A

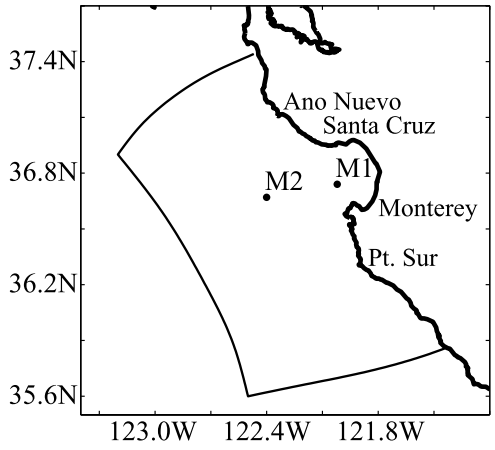

Figure 1. The Monterey Bay model domain with locations of moorings M1 and M2.

number of modifications were made to the physical parameterizations during a 5-year period that encompassed the advancement of COAMPSv2 to COAMPSv3. The two most important differences between the two versions of the COAMPS are related to the surface flux and microphysics parameterizations. In particular, the modified surface flux scheme improves the wind stress calculation as compared with observed values [*Wang et al.*, 2002]. Consequently, the new scheme significantly improves the near-surface wind prediction as the wind-speed bias is reduced by half during the daytime heating cycle over land areas. Additionally, improvements to the surface energy budget over land (including the soil moisture representation and deep soil parameterization) were introduced. The microphysics parameterization is formulated following *Rutledge and Hobbs* [1983]. A number of improvements were made to the microphysics including a new representation of the ice phase microphysics and a reformulation of the entire scheme in order to achieve total water conservation.

[14] COAMPS assimilates atmospheric observations from radiosondes, aircraft, satellite, and ships [*Hodur et al.*, 2002], The COAMPS SST analysis is performed directly on the particular nest grid and includes assimilation of observations from ships, buoys, satellites (for example, Multi-Channel Sea Surface Temperature (MCSST)). Atmospheric, as well as oceanic observations from moorings M1 and M2 (Figure 1) were not assimilated into the COAMPS simulations.

[15] The 3- and 9-km resolution nests from the COAMPSv3 version will be referred to as "3km, Cv3" and "9km, Cv3", respectively. The 9-km nest from the COAMPSv2 will be referred to as "9km, Cv2". All COAMPS products provide atmospheric fluxes with hourly frequency and the NCOM interpolates them to the current model time.

4. Brief Description of Observed Physical Conditions and COAMPS Predictions During 15 August–2 September 2000

[16] A plot of observed wind velocities at moorings M1 and M2 (Figure 1) is presented in Figure 2a. The plot indicates that during 15–21 August there was a strong upwelling favorable event, which was followed by a brief relaxation event of 22–23 August. Upwelling favorable winds resumed during 24–27 August. This brief upwelling event was followed by an extended relaxation event of 28 August–2 September 2000 [see also, *Ramp et al.*, 2005 and *Fitzwater et al.*, 2003]. Our major focus will be on the model's ability to reproduce the extended relaxation event of 28 August–2 September and the upwelling event of 17–21 August.

[17] During upwelling, cold offshore flowing filaments can be seen at two upwelling centers: north of the Monterey Bay around Pt. Año Nuevo, and south at Pt. Sur (Figure 1). In between these upwelling centers, there often exists a warm mesoscale eddy. The position of the eddy is observed to migrate onshore and offshore. The upwelling event of 17–21 August was characterized by the appearance of cold, salty water at Point Año Nuevo (Figure 1) which subsequently spread southward across the mouth of the bay as the winds continued. The circulation in the bay itself was cyclonic with very warm water observed in the northeast corner of the bay. During the wind relaxation event, the surface current and temperature response was dominated by the onshore translation of the offshore eddy and by local surface heating in the bay itself. Surface currents in the bay remained cyclonic.

[18] Plots of wind velocities from the different COAMPS products at stations M1 and M2 are presented in Figures 2b, 2c, and 2d. Figures 2b, 2c, and 2d also show the complex correlations (a) and angular displacements (theta) [estimated according to *Kundu*, 1976] between the observed wind velocity and the COAMPS-predicted wind velocities for the three products considered here. The angular displacement gives the average counterclockwise angle of the COAMPS wind velocity with respect to the observed wind velocity. All the COAMPS products show a correlation higher than 0.68 with the observed wind velocity at M1 and M2 and small angles of displacement. The correlation 0.68 is significant (different from zero) if the number of degrees of freedom is larger than or equal to 5 for a significance level of 0.05 (see for example, Table XI of *Hogg and Tanis* [1993]). The correlations on Figure 2 were calculated between the hourly COAMPS and observed wind velocities. Therefore around 432 samples were used to compute the correlations. It is clear that the number of degrees of freedom is smaller than 432, but we can assume that it is larger than 5 for the following reasons: two upwelling and two relaxation events are observed over the considered time frame; there is a strong diurnal variability in the atmospheric conditions in the area, and correlations over an 18-day time frame were estimated. At the same time, we cannot conclude that correlations on Figure 2 are significantly different due to uncertainty about the actual number of degrees of freedom and small differences between the correlations for the three considered COAMPS products.

[19] There is remarkable agreement between COAMPS predicted winds and observations in the sequence and extent of each upwelling-relaxation event observed during 15 August–2 September. However, at M1 there is an overestimation of wind velocity during the first upwelling for the "3km,Cv3" model run. The nearshore winds in "3km,Cv3" are probably amplified in comparison to "9km,Cv3" because of the better resolution of the terrain and coastline features. The coastal topography is steeper in

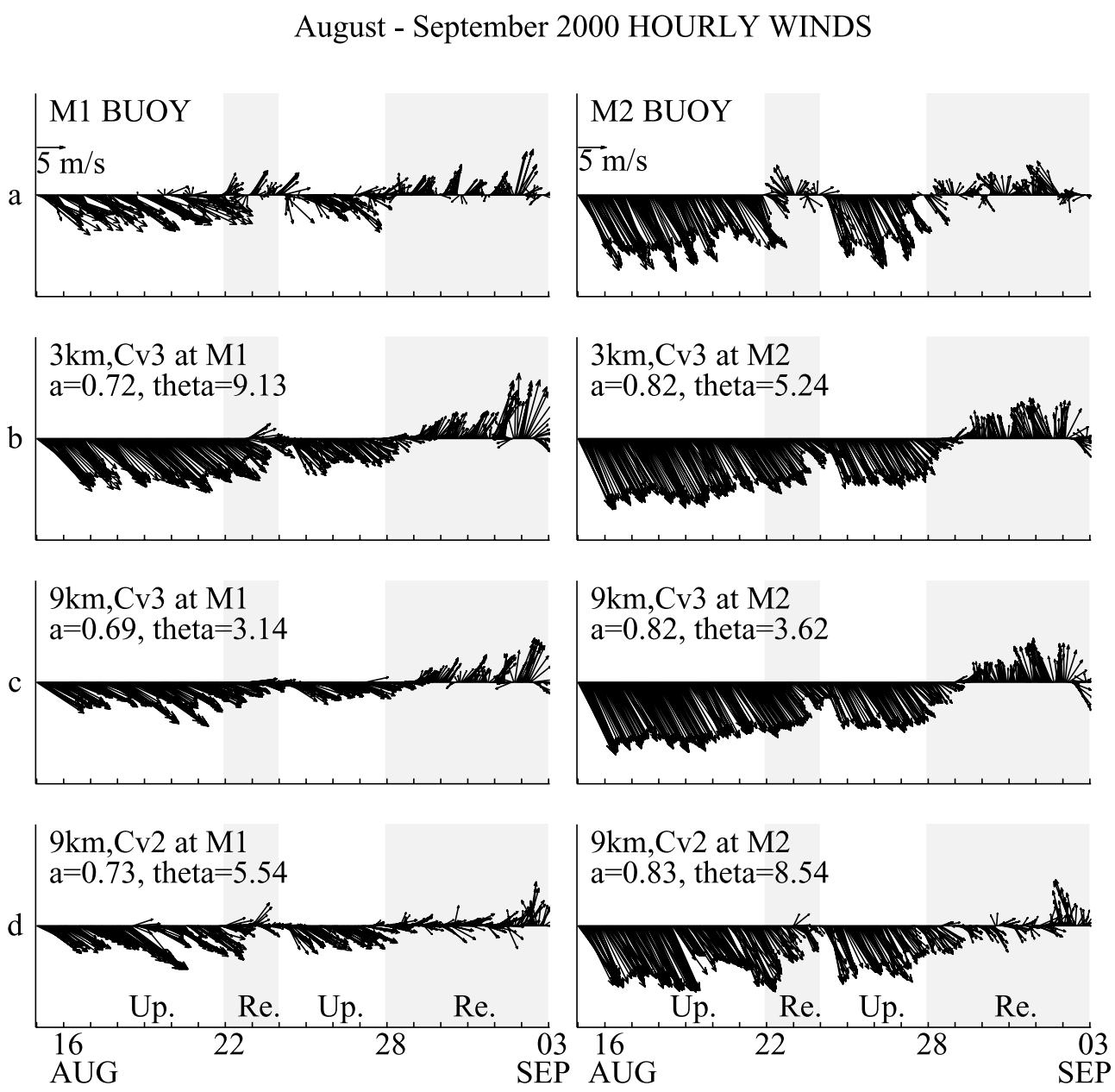

Figure 2. Observed and COAMPS model predicted wind velocities at M1 and M2: (a) observations; (b) COAMPS version 3 with 3-km resolution (3km,Cv3); (c) COAMPS version 3- with 9-km resolution (9km,Cv3); (d) COAMPS version 2 with 9-km resolution (9km,Cv2); Notations "Up." and "Re." mean upwelling and relaxation.

the 3-km mesh and can produce wakes and wakes flow regions with sharper gradients. This is particularly the case in the strong northwesterly flow regime in which the coastal terrain, such as the Santa Cruz Mountains, can force a lee-side wake. The acceleration as a result of the boundary layer flow around the headlands can be larger as well due to the steeper and better resolved terrain.

[20] Plots of daily averaged, photosynthetically available radiation (PAR) observed at M1 and M2 and estimated from the COAMPS short wave radiation (SWR) fluxes are presented in Figure 3a for M1 and Figure 4a for M2. The observed PAR was measured by the Biospherical PRR-620 spectroradiometer mounted on moorings approximately 3 m above the water surface [*Chavez et al.*, 2000]. PAR from COAMPS predictions was estimated as 45% of the COAMPS-predicted SWR flux [*Strutton and Chavez*, 2004]. Anomalies of the observed and model-predicted PAR values (deviations from the mean value over the considered time period) are plotted. Observed and model predicted mean values of PAR are shown in the upper left corner of each subfigure of Figures 3a and 4a.

[21] From the observed and model-predicted mean values presented in Figures 3a and 4a, it is clear that there is an overestimation of the SWR in the COAMPS predictions for all the COAMPS products considered here, especially for the "3km,Cv3" and "9km,Cv3" products. The excessive

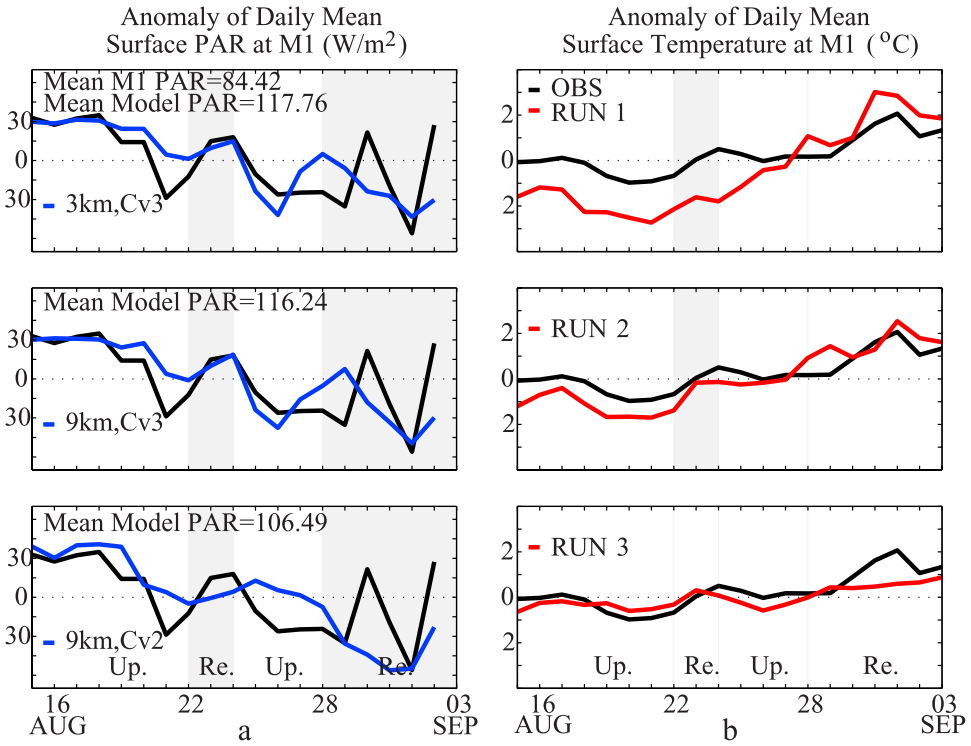

Figure 3. (a) Observed and the COAMPS-derived PAR anomalies at M1 location from three COAMPS products: 3km,Cv3; 9km,Cv3; and 9km,Cv2 (see captions of the Figure 2 for explanations of notations). (b) Observed and the model predicted SSTs from the NCOM ICON runs 1–3 (see Table 1) forced with corresponding COAMPS products shown on the left panels.

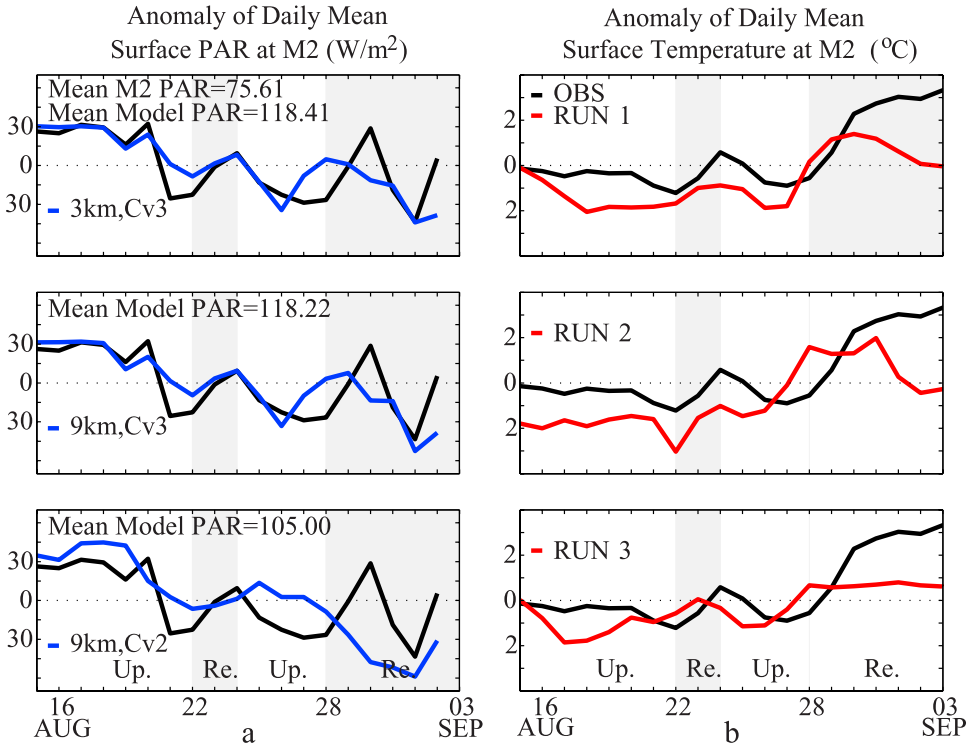

Figure 4. Same as Figure 3 but at mooring M2.

Table 1. Description of NCOM Runs

Runs	COAMPS Version	COAMPS Resolution	SWR Correction	Vertical Grid
Run 1	COAMPSv3	3 km	None	30 sigma layers
Run 2	COAMPSv3	9 km	None	30 sigma layers
Run 3	COAMPSv2	9 km	None	30 sigma layers
Run 4	COAMPSv3	3 km	Reduced by 75 W/m^2	30 sigma layers
Run 5	COAMPSv3	3 km	Reduced by a factor of 1.4	30 sigma layers
Run 6	COAMPSv3	9 km	Reduced by a factor of 1.4	30 sigma layers
Run 7	COAMPSv3	3 km	Reduced by a factor of 1.4	Hybrid, 40 layers (19 sigma, 21-*z*)
Run 8	COAMPSv3	9 km	Reduced by a factor of 1.4	Hybrid, 40 layers (19 sigma, 21-*z*)

SWR is likely related to a modeling of low-level clouds, which are very extensive during summer time in the Monterey Bay area. Accurate prediction of low-level clouds is a very challenging problem. We believe that the COAMPS model probably underestimates low-level clouds in the Monterey Bay area.

[22] Analysis of the anomalies presented in Figures 3a and 4a exhibits a good correspondence between the COAMPS-predicted and observed PAR, especially for the "3km,Cv3" and "9km,Cv3" products. The older version of the COAMPS "9 km,Cv2" run completely missed the local increase in SWR observed during the relaxation event of 27–31 August (see Figure 3a, bottom panel). As shown below, this missed event in the predicted SWR was one of the reasons why the POM ICON model was not able to reproduce the extraordinary surface heating within the bay during 30–31 August [*Ramp et al.*, 2005].

5. Results

[23] Table 1 describes attributes of the NCOM ICON runs evaluated in the paper. All the considered model runs were initialized on August 2 of 2000 by using fields from the same NCOM CCS model, which was forced with the "9km,Cv3"atmospheric forcing. NCOM ICON results during the 15 August–2 September are evaluated.

5.1. Sensitivity to the Resolution of the Atmospheric Forcing

[24] First, we compare the following NCOM ICON runs (see Table 1): run 1, the model is forced with "3km,Cv3"; run 2, the model is forced with "9km,Cv3"; and run 3, the model is forced with "9km,Cv2".

[25] Figures 3b and 4b present observed and model-predicted SST anomalies (deviations from the corresponding means over considered time frame) at moorings M1 and M2.

[26] The PAR observations at moorings (Figures 3a and 4a) show that the incoming solar radiation was the strongest during the extended upwelling event (15–21 August). This local heating interacted with cold, upwelled water from the northern upwelling center at Año Nuevo [*Ramp et al.*, 2005, Figure 1]. Little cooling is observed at M2 (Figure 4b), which is located in an area only weakly affected by the cold, upwelled water from the north (mostly moving along the entrance to and into the Bay between M2 and M1). Even at M1, the cooling at the surface takes place after 18 August when there is a reduction in the PAR (Figure 3a). On average, PAR during the first, brief relaxation event (22–23 August) is lower than during the upwelling, especially at the mooring M2 (Figure 4a). However, the strong increase of the daily SWR at the end of the upwelling and the beginning of the relaxation events (Figures 3a and 4a) leads to the increase of the surface temperatures at M1 and M2 during this brief period of relaxation (Figures 3b and 4b). This is followed by cooling during the brief upwelling event of 24–27 August. All three NCOM ICON runs were able to reproduce the above-described sequence of cooling and warming, especially at mooring M2 (Figure 4b). The model simulations during the extended relaxation period (28 August–2 September) will be discussed in detail in section 5.3.

[27] Statistics for runs 1–3 and for the observations at moorings M1 and M2 are presented in Table 2. Note that there are potential problems with the use of point-to-point comparisons with mooring observations for validation of the three dimensional circulation models. There are often spatial and temporal shifts between model predicted and observed features. As a result, relatively small spatial offsets in the modeled features can lead to an unrealistically poor assessment of model predictions when comparisons are done with the point mooring observations.

[28] All three runs show a high, larger than 0.7 correlation with observations. Following the discussion in section 4, the correlation 0.7 is significant if the number of degrees of freedom is larger than or equal to 5. All three runs have minimum, maximum, and mean values of temperature warmer than that observed at M1 and M2. This is a result of the overestimation of SWR fluxes in COAMPS predic-

Table 2. Surface Temperature Statistics 15 August–2 September

	M1					M2				
	Min	Max	Mean	SD	Correlation	Min	Max	Mean	SD	Correlation
OBS	11.11	15.02	12.54	0.84		11.46	16.62	13.46	1.36	
Run1	12.60	19.34	14.69	1.73	0.88	14.10	19.14	14.77	1.34	0.81
Run2	14.22	19.62	16.00	1.32	0.87	12.65	20.31	15.85	1.81	0.79
Run3	13.87	16.27	14.71	0.50	0.71	13.16	17.18	15.03	1.11	0.79
Run4	12.19	17.54	13.79	1.29	0.90	13.91	17.82	15.30	0.94	0.73
Run5	12.16	17.16	13.68	1.22	0.89	13.77	17.40	15.30	0.87	0.69
Run6	13.60	16.57	14.65	0.81	0.82	12.88	17.58	14.91	1.06	0.69
Run7	12.12	16.53	13.36	1.15	0.82	13.84	16.74	14.98	0.82	0.63
Run8	13.17	16.09	14.25	0.66	0.64	13.33	17.61	15.18	0.87	0.73

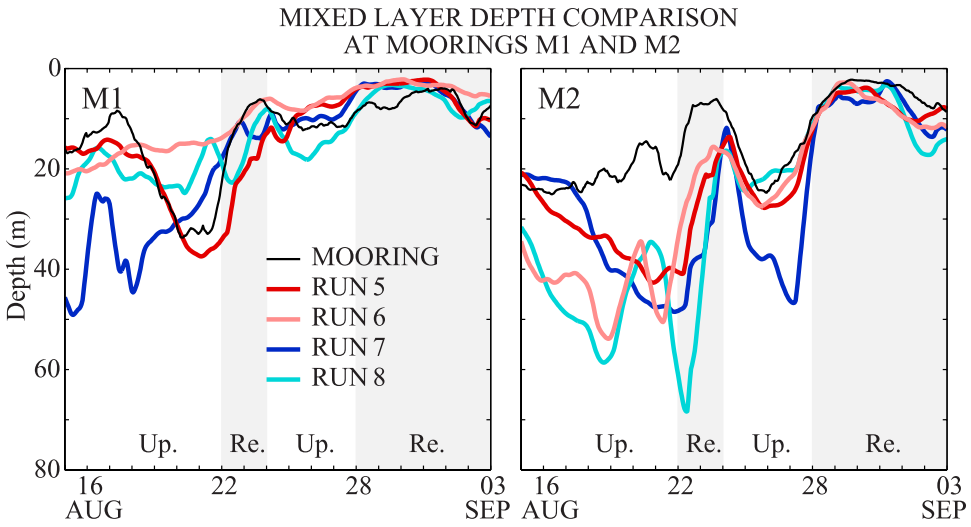

Figure 5. Observed and NCOM-ICON model predicted mixed layer depth (MLD) comparisons at M1 and M2.

tions. For example, in run 1, the mean temperatures are higher than the observed means by 2°C at M1, and by about 1°C at M2. The maximum and minimum values deviate even more strongly from the observed values. This directly correlates with the positive biases in the PAR values presented in Figures 3a and 4a. The mean PAR value for the "3km, Cv3" is around 118 W/m^2 at M1, which is about 1.4 times larger than the observed mean value of 84 W/m^2. In order to correct the temperature bias, two new runs were conducted in which the values of the SWR flux were adjusted to better match the observed values.

[29] Run 4 (Table 1) is a clone of run 1, but the COAMPS SWR fields were reduced by 75 W/m^2, which corresponds to a reduction in PAR of 34 W/m^2, which is equal to the difference between the COAMPS-derived and observed values of PAR at M1. Run 5 (Table 1) is a clone of run 1, but the COAMPS SWR fields were reduced by a factor of 1.4. In both runs, the mean of the SWR at M1 is near the observed value at M1. However, reduction by a factor of 1.4 will reduce the mean and variance in the SWR fields in run 5, while in run 4, only the mean value is reduced. Note that mean values of SWR in runs 4 and 5 are still higher than the observed values at M2. The statistics from runs 4 and 5 are presented in Table 2. The reduction in the COAMPS-predicted SWR significantly reduced the mean and maximum values of the NCOM model temperatures, while maintaining high correlation with the observed temperatures at M1 and M2. Based on the mooring observations, correction of the SWR forcing improves agreement between the observed and the NCOM ICON model-predicted SSTs.

5.2. Sensitivity to the Vertical Coordinate System

[30] In this section, we compare run 5 and three more runs (Table 1). Run 6 is a clone of run 2 but is forced with adjusted (divided by 1.4) SWR from the "9km,Cv3". Run 7 is a clone of run 5 (forced with "3km,Cv3" forcing), but the NCOM ICON model uses a hybrid coordinate system in the vertical (see section 2, the hybrid grid has 40 total vertical layers with 19 sigma layers and 21 z-levels). Run 8 is a clone of run 7 but is forced with "9km,Cv3" forcing. In both runs 7 and 8, SWR was adjusted as in runs 5 and 6. Therefore, comparisons of runs 5–8 will provide insight into the sensitivity of the model results to the vertical coordinate systems (sigma versus hybrid) under different resolution atmospheric forcing ("3km,Cv3" versus "9km,Cv3").

[31] SSTs statistics for runs 5–8 (presented in Table 2) are very similar with slightly better correlations for runs 5 and 6. Figure 5 provides comparisons of mixed layer depth (MLD) for runs 5–8. MLD is defined here as the depth at which the water temperature becomes 0.8° less than the SST [*Kara et al.*, 2000]. At M1, run 5 reproduced better the observed deepening/shallowing of the MLD during the upwelling/relaxation events than the other considered runs. This is reflected in the statistics presented in Table 3, where the correlations with the observed MLD and the root mean square (RMS) errors are shown for runs 5–8. The MLD for run 7 ("3km,Cv3" forcing, hybrid coordinate system) shows a noisy, oscillating MLD during strong upwelling (15–21 August, Figure 5). Run 6 ("9km,Cv3" forcing, sigma coordinates) missed the deepening of the MLD during this event (Figure 5). At M2, all the runs show a deeper than observed MLD during upwelling (15–21 August, Figure 5). This strong deepening in the model results might be an indication that, in the model predictions, upwelled water moves offshore too far by reaching the location of M2. Mixed results in the prediction of MLD at M2 are reflected in Table 3, where none of the runs shows better results.

5.3. Simulations During the Extended Relaxation Event

[32] Both runs 1 and 2 (forced with the new COAMPS "3km,Cv3" and "9km,Cv3" products) were able to reproduce the extreme warming during the extended relaxation event of 28 August–2 September, while run 3 (forced with the "9km,Cv2" run) missed this event (Figures 3b and 4b). One of the reasons for this is that the atmospheric forcing "9km,Cv2" does not have the observed increase in SWR during the relaxation event (Figures 3a and 4a). The "9km,Cv2" was also used to force the POM ICON run

Table 3. Comparisons of MLD Predictions

	RMS (m)		Correlation	
	M1	M2	M1	M2
RUN 5	5.5042	10.0535	0.79	0.54
RUN 6	6.0090	11.8851	0.52	0.64
RUN 7	10.7499	12.8919	0.54	0.49
RUN 8	6.4523	14.7254	0.55	0.56

described by *Ramp et al.* [2005] and, which also missed the strong temperature increase during the relaxation.

[33] As was speculated by *Ramp et al.* [2005], the offshore thermal maximum during the relaxation period at M2 is ascribed to a combination of advection and surface heating, but primarily advection, while within the inner bay (at M1), the thermal maximum was due to surface heating. This corresponds to *Rosenfeld et al.* [1994, page 954], where it is noted that a large surface temperature increase during the relaxation "cannot be accounted for by surface heat flux alone and must be result of advection".

[34] Figure 6 shows the two-dimensional structure of the wind stresses for the three COAMPS products averaged over the relaxation period. It is clear that the "9km,Cv2" run has a different structure than the "3km,Cv3" and "9km,Cv3" runs. As a result, the offshore California current warm water was advected more onshore during the relaxation in runs 1 and 2 with the "3km,Cv3" and "9km,Cv3" forcing when compared to run 3 with the "9km,Cv2" forcing (Figure 7). This is another reason why runs 1 and 2 reproduce the strong temperature increase and run 3 does not. Note that the "3km,Cv3" and "9km,Cv3" wind velocities agree better with the aircraft-observed wind velocity [see Figure 8 in *Ramp et al.*, 2005].

[35] Heat contents changes for runs 1–3 were estimated during the observed surface heating event of 30–31 August. The area of the bay bounded on the west by the section crossing the location of the mooring M1 (Figure 1), and going along the entrance to the bay from Santa Cruz at the north to Monterey in the south, was considered in the heat analysis. During 30–31 August, changes in the heat content due to SWR for NCOM runs 1 and 2 (forced with the COAMPSv3) are about 30% larger than run 3 (forced with COAMPSv2). Note, that flux due to SWR is around 3.5 times larger than the total flux of the other three: latent, sensible, and long wave radiation heat fluxes. During 30–31 August, the change of heat content due to advection (for the top 15 m) is about 3.5 times larger for run 1, and about 2 times larger for run 2 in comparison to run 3. This supports above findings, in that the missed increase in SWR and the deficiency in wind stress structure for the COAMPSv2 product resulted in the inability of the NCOM ICON run 3 and the POM ICON run to reproduce the observed extreme local heating during the relaxation period.

5.4. Simulations During the Extended Upwelling Event

[36] Figure 8 presents wind stresses averaged over the upwelling period (15–21 August) for the "3km,Cv3" and "9km,Cv3" products. The corresponding averaged circulation patterns for run 5 (forced with "3km,Cv3") and run 6 (forced with "9km,Cv3") are shown in Figure 9. Both runs reproduced the observed upwelling at Pt. Año Nuevo and Pt. Sur (Figure 9). At the same time, the "3km,Cv3" wind stress is stronger than the 9-km stress near the coast (Figure 8). This generates stronger upwelling in run 5 than in run 6. The southward jet, between the warmer water of the California Current and the upwelled water, flows along the entrance to the bay in run 5. This agrees with observations from *Ramp et al.* [2005] and the CODAR-observed surface currents presented in Figure 10 (left panel). In run 6, the surface current flows offshore and then flows along the bay.

[37] Run 6 shows a northward flow along the coast that emanates from the southern open boundary of the model domain. This northward flow is not present in run 5. Note that during the relaxation period (Figure 7), a northward flow at the surface is present in both runs 1 and 2 (and in runs 5 and 6, not shown here). During relaxation, when the wind forcing is weakening, the northward flow develops and this flow is well observed [*Ramp et al.*, 2005]. The

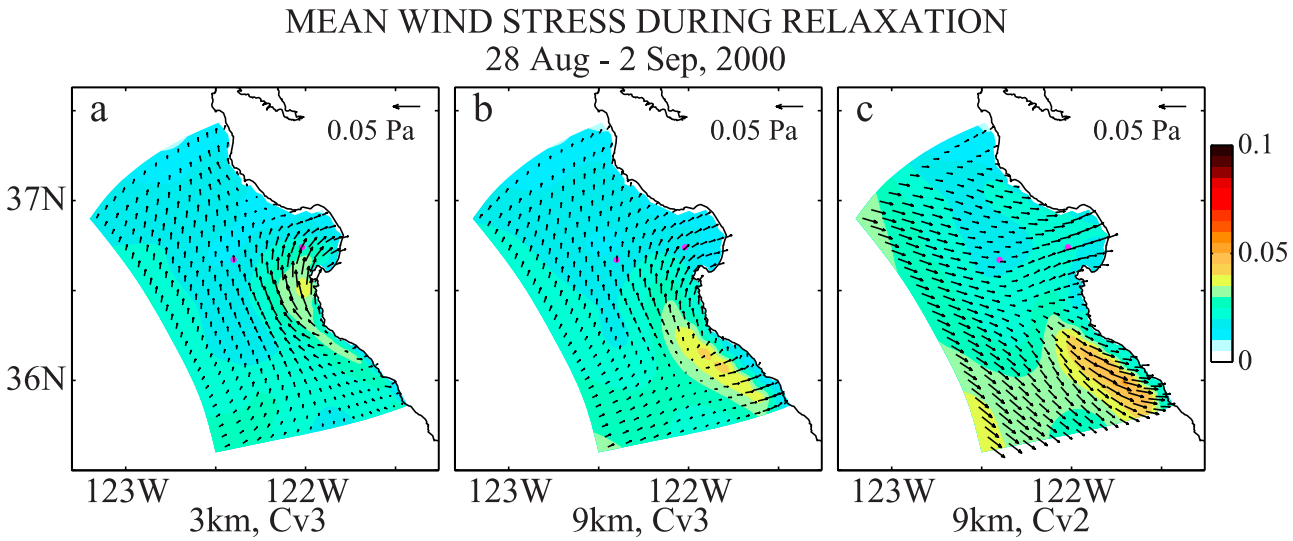

Figure 6. Averaged over the relaxation event wind stresses from three COAMPS products: (a) −3km,Cv3; (b) −9km,Cv3, and (c) −9km,Cv2. See captions of Figure 2 for explanations of notations.

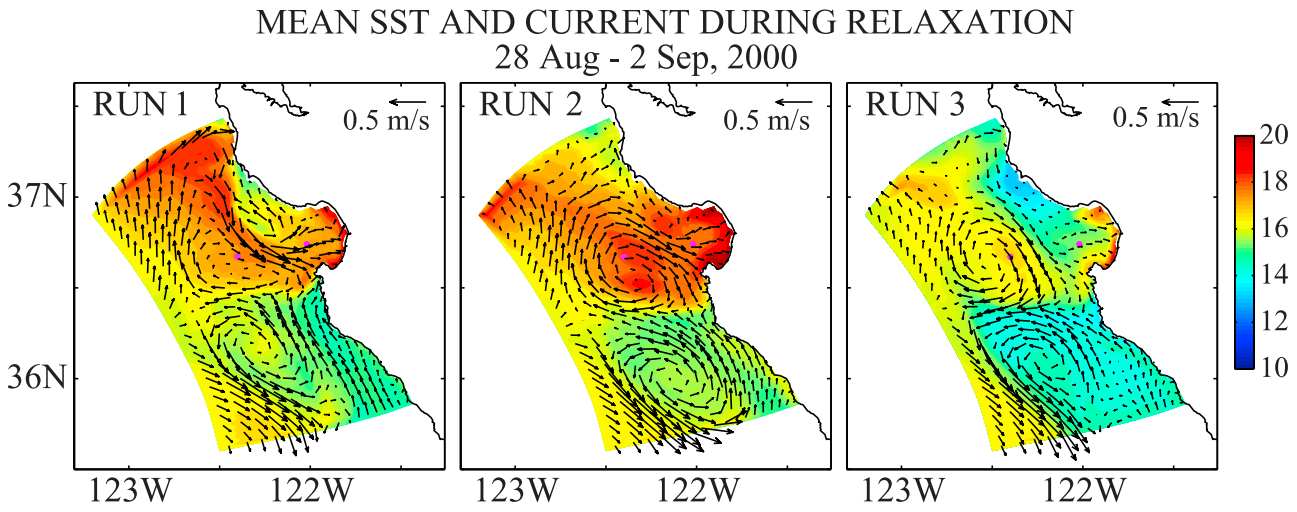

Figure 7. The NCOM ICON model predicted SSTs (averaged over the relaxation event) from runs 1–3 (Table 1) forced with corresponding COAMPS wind stresses from the Figure 6.

question is whether the surface northward flow shown in run 6 during the upwelling (strong winds) is a physical phenomenon, especially since run 5, which differs only in having higher-resolution atmospheric forcing, does not reproduce this aspect.

[38] The CODAR radial currents observed at Pt. Sur and averaged over the same upwelling event (Figure 10, right panel) show a southward flow at Pt. Sur, which corresponds to the results of run 5 but not run 6. Therefore, we should conclude that the development of northward flow at the surface during the upwelling in run 6 is unrealistic. What is the reason for the development of this artificial northward flow? Figure 11 shows the NCOM CCS velocity normal to the southern open boundary of the NCOM ICON domain. The NCOM CCS velocity is averaged over the upwelling event. Positive values indicate northward flow, and negative values indicate southward flow. Figure 11 demonstrates that the NCOM CCS velocity has southward flow at the surface close to the coast. Therefore, open boundary conditions at the southern boundary of the NCOM ICON model are not responsible for the development of the northward flow in the NCOM ICON run 6.

[39] Comparison of the wind patterns of the "3km,Cv3" and "9km,Cv3" products (Figure 8) shows the weakening of the "9km,Cv3" wind stress along the southern coast of the NCOM ICON model domain. As indicated by *Capet et al.* [2004], this weakening or drop off at the coast is a source for intensification of the northward flow south to Pt. Sur (as

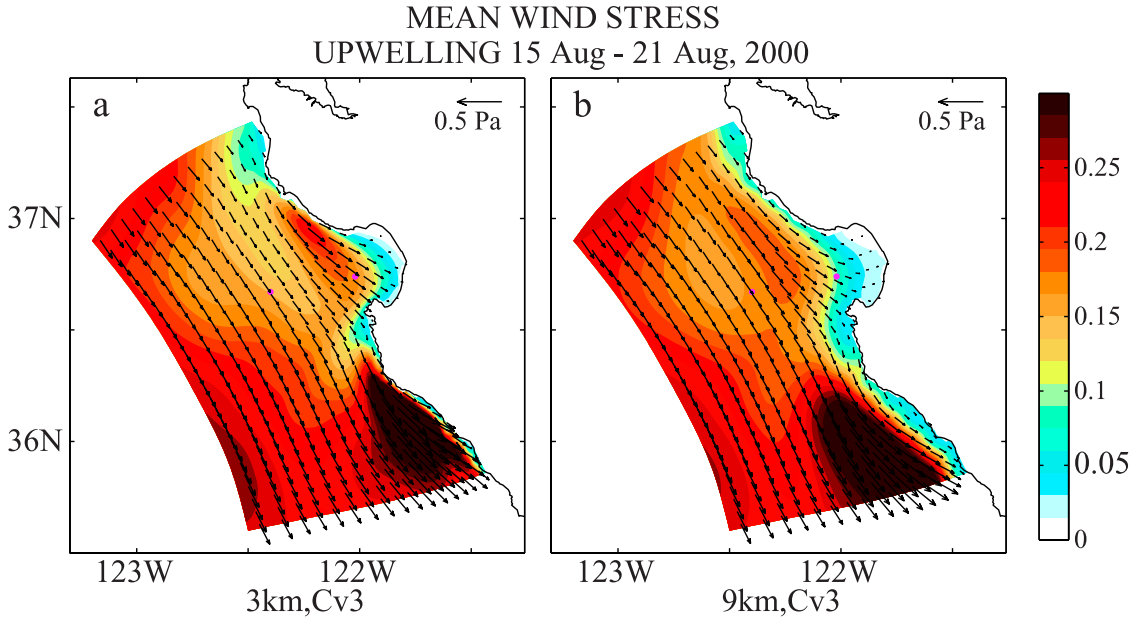

Figure 8. Averaged over the upwelling event wind stresses from two COAMPS products: (a) −3km,Cv3 and (b) −9km,Cv3.

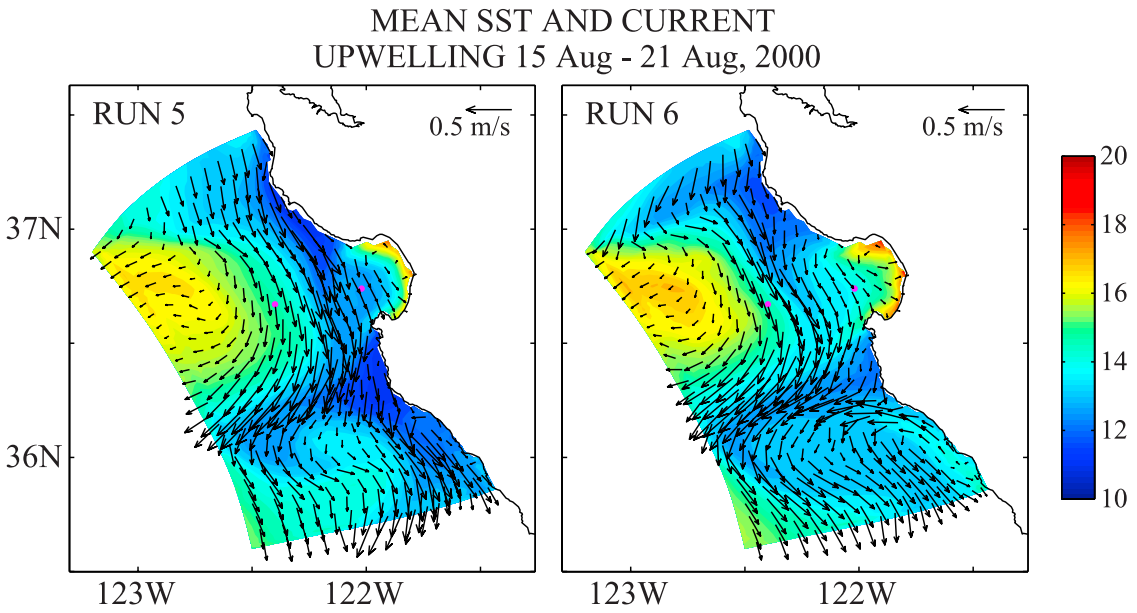

Figure 9. The NCOM ICON model predicted SSTs (averaged over the upwelling event) from runs 5 and 6 (Table 1) forced with corresponding COAMPS wind stresses from the Figure 8.

it is seen in run 6). Therefore the reason for the development of the artificial northward flow in run 6 is the weakening of the 9km COAMPS wind at the coast in the southern portion of the domain. The impact of high-resolution wind fields on the POM ICON model results were studied by *Blencoe* [2001].

6. Discussions and Conclusions

[40] Results from the NCOM-based model (NCOM ICON) of the Monterey Bay area are evaluated during 15 August–2 September 2000. The time frame includes an extended upwelling event during 15–21 August and an extended wind relaxation event from 28 August through 2 September.

[41] The atmospheric fields from two COAMPS versions (the older version COAMPSv2 and the newer version COAMPSv3) are compared to observed wind and PAR values at moorings M1 and M2. COAMPS predicted winds show a good agreement with observations in the sequence and extent of each upwelling-relaxation event observed during 15 August–2 September 2000. As a result, the NCOM ICON runs forced with both COAMPS versions were able to reproduce the sequence of the observed upwelling/relaxation events.

[42] However, comparison of the observed and COAMPS estimated PAR values show that there is overestimation of

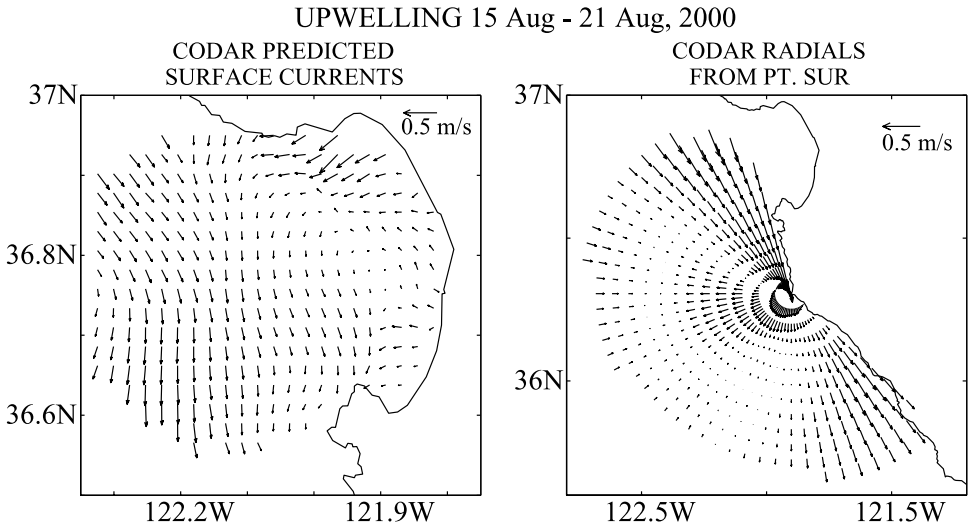

Figure 10. Averaged over the upwelling event CODAR derived surface currents (left) and radials at Pt. Sur (right).

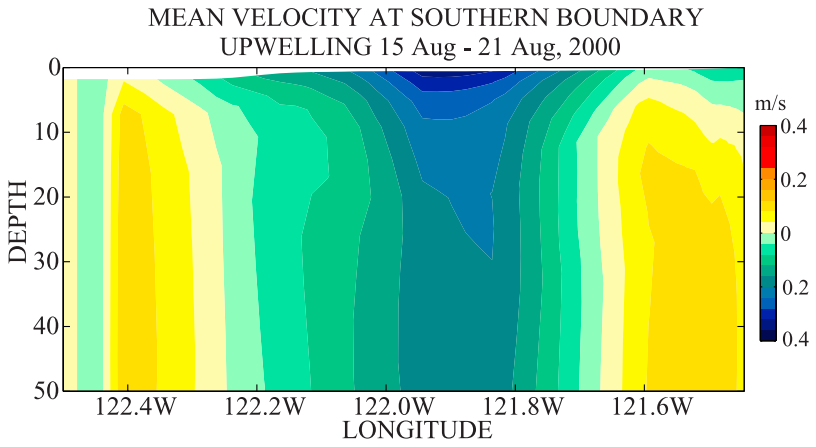

Figure 11. The NCOM CCS alongshore velocity plotted along the southern open boundary of the NCOM ICON model. The velocity is averaged over the upwelling event. Positive values mean northward flow.

SWR (by around 40%) in the COAMPS predictions. The excessive SWR is likely related to a modeling of low-level clouds, which are very extensive during summer time in the Monterey Bay area. As a result of the overestimation of SWR, the NCOM ICON model results show minimum, maximum, and mean values of temperature warmer than that observed at M1 and M2. In order to correct the temperature bias, the NCOM ICON runs were conducted with the values of the COAMPS SWR flux adjusted to better match the observed values. It is shown that the correction in the COAMPS-predicted SWR significantly reduced the mean and maximum values of the NCOM model temperatures, while maintaining high correlation with the observations at M1 and M2. These results demonstrate that the correction of the atmospheric model SWR based on the mooring observations improves the agreement between the observed and the NCOM predicted SSTs at the mooring locations.

[43] The NCOM ICON runs forced with different resolution atmospheric forcing (3- versus 9-km resolution) as well as the NCOM ICON runs employing different vertical coordinate systems (sigma versus hybrid) do not show significant differences in the prediction of SST (Table 2). However, comparisons of mixed layer predictions show that the run 5, with a sigma vertical coordinate system and forced with 3-km resolution forcing, better reproduced the observed deepening/shallowing of the MLD during the upwelling/relaxation at the M1 mooring location. At mooring M2, all the runs show a deeper than observed MLD during upwelling (15–21 August). This strong deepening might be an indication that, in the model results, upwelled water moves offshore too far by reaching the location of M2. Mixed results in the prediction of MLD at M2 are reflected in Table 3, where none of the runs show better results.

[44] During the wind relaxation event (28 August–2 September), strong onshore translation of warmer California Current water combined with local surface heating inside the bay resulted in extraordinary surface warming within the bay. As reported by *Ramp et al.* [2005], the POM ICON model simulations forced with the older version of the atmospheric model COAMPS (COAMPSv2) were not able to reproduce this observed extraordinary surface warming. Similarly, the NCOM ICON run forced with the same version of the COAMPS missed the event. Analysis of the COAMPSv2 atmospheric fields show two reasons for this: the missed observed increase in SWR during the relaxation event and the deficiency in wind stress structure, which does not bring offshore warmer water into the Bay. However, the NCOM ICON model runs forced with the new COAMPSv3 fields (3- and 9-km resolution) were able to reproduce the observed event.

[45] During the extended upwelling event, the NCOM ICON runs forced with 3- and 9-km resolution COAMPSv3 fields (runs 5 and 6, Table 1), respectively, show differences in surface circulation patterns. The most distinct difference is in the southern portion of the NCOM ICON model domain: the run forced with 9-km forcing shows the northward flow along the coast that emanates from the southern open boundary of the model domain. This northward flow is not present in the run forced with 3-km forcing. Observations like CODAR radials, as well as predictions from the larger scale California Current model (NCOM CCS predictions which are used on open boundaries of the NCOM ICON model), show southward flow in the southern portion of the model domain. Comparison of the wind patterns of the 3- and 9-km products (Figure 8) shows the weakening of the 9-km wind stress along the southern coast of the NCOM ICON model. This weakening is responsible for the development of the artificial northward flow in the NCOM ICON run. The weakening of the 9-km wind stress at the coast is also indicated as a source for intensification of northward flow in the work of *Capet et al.* [2004].

[46] **Acknowledgments.** This research was funded through the Naval Research Laboratory (NRL) under Program Element 61153N sponsored by the Office of Naval Research. Our thanks to Mike Cook and Fred Bahr of NPS for providing assistance with the quality control, processing, and presentation of the CODAR and mooring data respectively. Computer time for the numerical simulations was provided through a grant from the Department of Defense High Performance Computing Initiative. Computational resources for COAMPS were supported in part by a grant of HPC time from the Department of Defense Major Shared Resource Centers, Aberdeen, MD and Wright Patterson Air Force Base, OH. COAMPS(r) is a

registered trademark of the Naval Research Laboratory. This manuscript is NRL contribution 7330-05-6050.

References

Blencoe, D. G. (2001), Impact of high resolution wind fields on coastal ocean models, M.S. thesis, 71 p, Naval Postgraduate School, Monterey, CA.

Blumberg, A., and G. L. Mellor (1987), A description of a three-dimensional coastal ocean circulation model in *Three Dimensional Coastal Models*, edited by N. S. Heaps, Coastal Estuarine Sci., 4, p. 1–16, AGU, New York.

Capet, X. J., P. Marchesiello, and J. C. McWilliams (2004), *Geophys. Res. Lett.*, *31*, L13311, doi:10.1029/2004GL020123.

Chavez, F. P., D. Wright, R. Herlien, M. Kelley, F. Shane, and P. G. Strutton (2000), A device for protecting moored spectroradiometers from biofouling, *J. Atmos. Oceanic Technol.*, *17*, 215–219.

Fitzwater, S. E., K. S. Johnson, V. A. Elrod, J. P. Ryan, L. J. Coletti, S. J. Tanner, R. M. Gordon, and F. P. Chavez (2003), Iron, nutrient and phytoplankton biomass relationships in upwelled waters of the California coastal system, *Cont. Shelf Res.*, *23*, 1523–1544.

Fox, D. N., C. N. Barron, M. R. Carnes, M. Booda, G. Peggion, and J. Van Gurley (2002), The modular ocean data assimilation system, *Oceanography*, *15*(1), 22–28.

Haidvogel, D. B., J. Blanton, J. C. Kindle, and D. R. Lynch (2000), Coastal ocean modeling: Processes, and real-time systems, *Oceanography*, *13*(1), 35–46.

Hodur, R. M., J. Pullen, J. Cummings, X. Hong, J. D. Doyle, P. J. Martin, and M. A. Rennick (2002), The Coupled Ocean/Atmospheric Mesoscale Prediction System (COAMPS), *Oceanography*, *15*(1), 88–98.

Hogg, R. V., and E. A. Tanis (1993), Probability and Statistical Inference, 731 p., Prentice-Hall, Upper Saddle River, N. J.

Kara, A. B., P. A. Rochford, and H. E. Hulburt (2000), An optimal definition for ocean mixed layer depth, *J. Geophys. Res.*, *105*, 16,803–16,821.

Kindle, J. C., R. Hodur, S. deRada, J. Paduan, L. K. Rosenfeld, and F. P. Chavez (2002), A COAMPS^{TM} reanalysis for the eastern Pacific: Properties of the diurnal sea breeze along the central California coast, *Geophys. Res. Lett.*, *29*(24), 2203, doi:10.1029/2002GL015566.

Kundu, P. K. (1976), Ekman veering observed near the ocean bottom, *J. Phys. Oceanogr.*, *6*, 238–242.

Martin, P. J. (2000), Description of the Navy Coastal Ocean Model Version 1.0, NRL/FR/732-00-9962, Naval Research Laboratory, Stennis Space Center, Mississippi.

Paduan, J. D., and I. Shulman (2004), HF radar data assimilation in the Monterey Bay area, *J. Geophys. Res.*, *109*, C07S09, doi:10.1029/2003JC001949.

Ramp, S. R., J. D. Paduan, I. Shulman, J. Kindle, F. L. Bahr, and F. Chavez (2005), Observations of upwelling and relaxation events in the northern Monterey Bay during August 2000, *J. Geophys. Res.*, *110*, C07013, doi:10.1029/2004JC002538.

Rhodes, R. C., et al. (2002), Navy real-time global modeling systems, *Oceanography*, *15*(1), 29–43.

Rochford, P. A., and I. Shulman (2000), Boundary Conditions in the Pacific West Coast Princeton Ocean Model of CoBALT. *NRL Tech. Rep.*, NRL/MR/7330-00-8245, 18 pp.

Rosenfeld, L. K., F. B. Schwing, N. Garfield, and D. E. Tracy (1994), Bifurcated flow from an upwelling center: A cold water source for Monterey Bay, *Cont. Shelf Res.*, *14*, 931–964.

Rosmond, T. E., J. Teixeira, M. Peng, T. F. Hogan, and R. Pauley (2002), Navy Operational Global Atmospheric Prediction System (NOGAPS): Forcing for ocean models, *Oceanography*, *15*, 99–108.

Rutledge, S. A., and P. V. Hobbs (1983), The mesoscale and microscale structure of organization of clouds and precipitation in midlatitude cyclones: VIII. A model for the "seeder-feeder" process in warm-frontal rainbands, *J. Atmos. Sci.*, *40*, 1185–1206.

Shulman, I., C. R. Wu, J. K. Lewis, J. D. Paduan, L. K. Rosenfeld, J. C. Kindle, S. R. Ramp, and C. A. Collins (2002), High resolution modeling and data assimilation in the Monterey Bay area, *Cont. Shelf Res.*, *22*, 1129–1151.

Shulman, I., J. Kindle, S. Derada, S. Anderson, B. Penta, and P. Martin (2004), Development of hierarchy of different resolution models for study U.S. West Coast California Current Ecosystem, in *Estuarine and Coastal Modeling*, edited by M. L. Spaulding, Proceedings of 8th International Conference on Estuarine and Coastal Modeling, p. 74–88.

Strutton, P. G., and F. P. Chavez (2004), Biological heating in the equatorial Pacific: Observed variability and potential for real-time calculation, *J. Clim.*, *17*, 1097–1109.

Wang, S., Q. Wang, and J. Doyle (2002), Some improvement of Louis surface flux parameterization paper presented at 15th Symposium on Boundary Layers and Turbulence, Am. Meteorol. Soc., 15–19 July 2002, p. 547–550, Wageningen, Netherlands.

S. Anderson, J. Kindle, P. Martin, B. Penta, and I. Shulman, Oceanography Division, Naval Research Laboratory, Stennis Space Center, MS 39529, USA. (igor.shulman@nrlssc.navy.mil)

F. Chavez, MBARI, 7700 Sandholdt Road, Moss Landing, CA 95039, USA.

S. deRada, Jacobs Sverdrup, Stennis Space Center, MS 39529, USA.

J. Doyle, Marine Meteorology Division, Naval Research Laboratory, Monterey, CA 93943, USA.

J. Paduan and S. Ramp, Department of Oceanography, Naval Postgraduate School, Monterey, CA 93943, USA.